Proceedings of ASME 2012 International Mechanical Engineering Congress & Exposition
IMECE 2012
November 11-14, 2012, Houston, Texas, USA

IMECE2012-86446

AERODYNAMIC INSTABILITY MODES FOR A LOAD SLUNG FROM A HELICOPTER

Sumant Sharma, Narayanan Komerath, Marilyn Smith and Vrishank Raghav
Daniel Guggenheim School of Aerospace Engineering
Georgia Institute of Technology
Atlanta, Georgia 30332
Email: ssharma46@gatech.edu

ABSTRACT

The aerodynamic-dynamic interaction of a load slung from a helicopter in flight can lead to divergent oscillations. In this paper, interactions between degrees of freedom are explored through fundamental simulation and wind tunnel experiments of generic shapes. Video analysis of the behavior of loads in a wind tunnel provides insights into dynamic behavior, and reveals the difference in behavior of the same model between wind tunnels of different sizes. A compound pendulum motion in a plane orthogonal to a steady freestream is first studied. Even with proximate walls, a purely symmetric single degree of freedom oscillation does not amplify. The addition of an out-of-phase force as a simplified model for yaw effects, leads to amplification or damping under some conditions. Wall effects amplify this interaction further. This level of simulation enables guidance to develop metrics for unsteady wall interference in dynamic testing. Results to-date set the context for future work in refining the aerodynamic and dynamic models, including tether and vehicle dynamics. Incorporation of quasi-steady and unsteady loads data from wind tunnel measurements and computational fluid dynamics would enable prediction of the linear superposition stage leading towards divergence. Comparison of simulaiton results to measured parameters from wind tunnel experiments shows relative agreement.

Nomenclature

α	Section lift coefficient
$\ddot{\theta}$	Angular Acceleration
$\overrightarrow{r_{pc}}$	Displacement vector of P from center of mass C
ρ	Density of freestream
θ	Angular Displacement
a_p	Acceleration of point P
A_{ref}	Surface area of box parallel to wind tunnel walls
C_p	Coefficient of Pressure
F	Normal coefficient
g	Acceleration due to gravity
I_{zz}^P	Moment of Inertia for load at point P along Z-Z axis
I_{zz}	Moment of Inertia for load along Z-Z axis
k	Doublet strength
l	Sling length
M_P	Moment balance at point P
m_T	Total mass of body
n	Scaling factor
q	Dynamic pressure
U_∞	Freestream velocity
V_θ	Orthogonal component of pendulum velocity
V_R	Radial component of pendulum velocity

INTRODUCTION

Rotorcraft are required to transport a wide variety of loads and cargo by means of external suspension. In many cases, the slung loads are suspended from the vehicle at a single point, allowing for a wide range of dynamics. Typical loads are aerodynamically bluff bodies comprised of various shapes and sizes. Steady and unsteady flow separation and turbulent wakes are usually encountered. The aerodynamic-dynamic interaction of these bodies is important because it can lead to large oscillations that can impose safety limits on both the loads and the vehicle.

In many applications where such loads are carried, speed is essential, whether to minimize exposure in zones with adverse weather or enemy presence, or to maximize rate of operations where lives must be saved from imminent danger. In forest fires, rising floodwaters, rescue from avalanches, mudslides and ocean disasters, the ability of helicopters to lift and transport slung loads swiftly is of critical importance. At the same time, the safety of the craft and the load are critical concerns. Thus, the maximum speed of safe operation is a critical parameter for the crew to know. Certifying each load-vehicle combination over the entire flight envelope is a daunting task, so more efficient and accurate techniques must be found to at least identify regions of concern for further detailed studies. The number of different phenomena, and the intricate details and texture of their behavior, become far too complex to allow good human insight into the mechanisms leading up to divergence. A simpler representation framework is desirable as a first step, with the capability to incorporate the details into this framework.

The primary emphasis of the work reported in this paper is to explore a quick and inexpensive method to identify how divergence might occur, at a fundamental mathematical level, representing forces and moments as elementary forms. This can potentially provide insight, and the ability to experiment with many combinations to represent various interaction mechanisms as building blocks. The detailed aerodynamic and dynamic properties may be added on later, with the basic knowledge gained from this exploration. In the hands of an expert engineer, this can become a powerful tool to gain and use physical insight, with a consistent mathematical framework.

The goal is to capture the spectrum of coupled unsteady aerodynamic–dynamic behavior encountered by loads tethered from helicopters by narrowing down to different sources and analysing their interaction. A fundamental simulation of divergence mechanisms would enable confident prediction of the performance of such loads at different speeds and sizes. The long-term goal is to develop a systematic understanding of the safe flight envelope for any given load/vehicle combination.

The present focus is to study the fundamental mechanisms that lead to divergence from stability. Yaw oscillations accompanying roll and pitch, are a big factor as seen from the video analysis of wind tunnel experiments. Some issues studied in this paper are:

1. Results from the two tunnels using the same CONEX 1/11 scale model yielded drastically different behavior. Is there a dynamic wall effect that amplifies the motion of the model?
2. Can this wall effect be simulated by simple aerodynamic/dynamic modeling?
3. Is it possible to simulate the processes leading to divergence using basic dynamics?
4. Will this level of simulation yield divergence?
5. Are the conditions of divergence realistic in the helicopter sling load context?

Prior Work

The variety of slung loads carried by military helicopters can be glimpsed from the Multiservice Manual for rigging loads for one kind of suspension [1]. Researchers around the world have studied the aerodynamics and stability of slung loads. The trailing angle of a slung load can be approximated to good accuracy using empirical drag estimation techniques, for instance using the classical work by Hoerner [2]. The wakes and drag of bluff body shapes have been studied by several researchers, for instance Wei [3] and Nakamura [4]. Lee [5] has studied the effect of aspect ratio on turbulent drag of rectangular bluff bodies. Gerrard [6], Barnes [7], Bearman [8], Bentley [9], King [10], Komatsu [11], and Matsumoto [12] describe vortex shedding from bluff bodies of various shapes.

Micale [13] presented a method of stabilizing slung loads using a rotating wheel. Rosen [14] described the correlation of flight test results on slung loads to scale model tests in a low speed wind tunne and showed that for cases with sharp-edged separation such as a rectangular container, results were scaleable, despite the large difference in Reynolds Number. A cube geometry as well as the standard rectangular CONEX container were discussed. Theron et al. [15] performed computational fluid dynamics calculations of the aerodynamics of slung loads, comparing wind tunnel and computed results. Cicolani et al. [16] reported on wind tunnel and flight experiments, and simulation of techniques for passive stabilization of slung loads. Raz et al. [17] cites that the maximum flight speed of a UH-60 with a Container Express (CONEX) cargo container slung load is 60 kts, as compared to the power-limited speed of 110 kts of that particular configuration. Reddy [18] presented simulation results on helicopter slung loads. They used the ROTGEN simulation environment to perform detailed 6-dof dynamics simulation of a helicopter-load system, based on the methods of Cicolani et al [19]. The center of gravity location of the load was varied to examine effects on dynamics. Greenwell [20] has surveyed the characteristics of the quasi-steady aerodynamic loads on various shapes, including flow separation characteristics, for use in predicting sling-load aerodynamics and dynamics.

Approach

The broad spectrum of slung loads can be in various complex profiles but they can be classified into six different generic shapesas shown in Tab. 2 in order to analyze different modes of instability. Each of these shapes is associated with different types of aerodynamic behavior and can be studied

TABLE 1. CLASSIFICATION OF SHAPES.

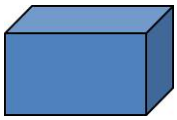 Box	 Cylinder
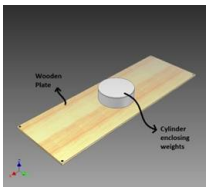 Flat Plate	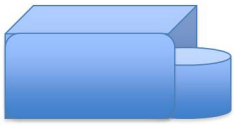 Combination
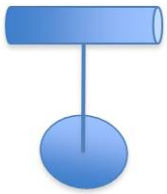 Double Load	 Basket

and simulated individually to narrow down the effects of their particular instability modes. The starting point is the flow around a rectangular box that experiences sharp-edge separation. There is a large body of validation data linking from small-scale wind tunnel experiments to full-scale flight experiments on the CONEX and other standard containers, as well as computational fluid dynamics. In the case of a circular cylinder the flow is subject to smooth separation, and in the case of a flat plate the flow will produce lift force for varying angles of pitch. Other shapes combining several of these features are a combination of the first three shapes in the form of a vehicle like an ambulance, a double load representing, for instance, a howitzer and ammunition, and a low density basket where flow is allowed to pass through. Along with their unique flow features, all these shapes also experience vortex shredding.

Results from wind tunnel testing and computational fluid dynamics on models of the CONEX and of cylinders of aspect ratio 1.0 at the John J. Harper wind tunnel facility (Georgia Institute of Technology) are described in [21,22]. The former dealt with dynamic wind tunnel test results on drag and instability of a CONEX and an aspect ratio 1 cylinder model, quasi-steady 6-dof load measurements in a wind tunnel, and computational fluid dynamics prediction of the CONEX loads. The latter added results from hot-film probe anemometry to gauge wake spectra, and comparisons with computational fluid dynamics, around a quasi-steady CONEX model placed on a 6 dof load cell.

During the course of those experiments, different variations of the scaled down CONEX container (box) were tested in the 7 x 9 ft. John J. Harper wind tunnel facility as well as the 42" (test section) wind tunnel at Georgia Institute of Technology. To model the dynamic behavior of the box, the load was tethered in a pendulum-like fashion. Four slings were attached at the four corners of the box and were designed out of 3.18 mm (1/8 in) thick rigid steel rods to provide minimum interference. A $1/11^{th}$ scaled model of a CONEX container of approximately 6 x 6 x 8 ft. weighing 4352 lbs at full scale, was examined. Linear dimensions were scaled proportional to the scaling factor n, the mass proportional to n^3, frequency proportional to $1/\sqrt{n}$, and velocity proportional to $\sqrt{n}$.

Initial experiments conducted by the team used flexible tethers (strings) rather than the rigid links used in scale-model experiments elsewhere. With flexible tethers, it is not possible to obtain the dynamics of the load from encoder readings at the gimbal mount where the load is slung. Instead, the initial assignment of the author was to analyze video image sequences of load behavior, in order to reconstruct time traces of the motion. To validate the accuracy of the process, a direct comparison was made with a later case where rigid tether links were used, and gimbal-mounted encoder data were also obtained. The results are shown in Fig. 1 below. Here automated MATLAB coding was used to determine the trailing angle through frame-by-frame analysis. These results proved to be quite accurate for the purposes of estimating drag on the model, as shown in Fig. 2 where the video analysis results are validated against encoder readings.

At lower speeds the box was observed to switch from the narrow side facing the flow to the broad side facing the flow. At higher speeds one of the main observations was the spinning behavior experienced by the load; these observations were made in both the tunnels. However, one major difference was the large roll oscillations accompanied with yaw which were only seen in the 42" tunnel and this motion was amplified at low speed. The divergence speed measured in the 42" tunnel was thus substantially lower than that seen from tests in the 7' x 9' tunnel. It must be noted that there was no rotor wake present in either case, so a major source of initial disturbance, triggering both yaw and roll oscillations, was absent when compared to an

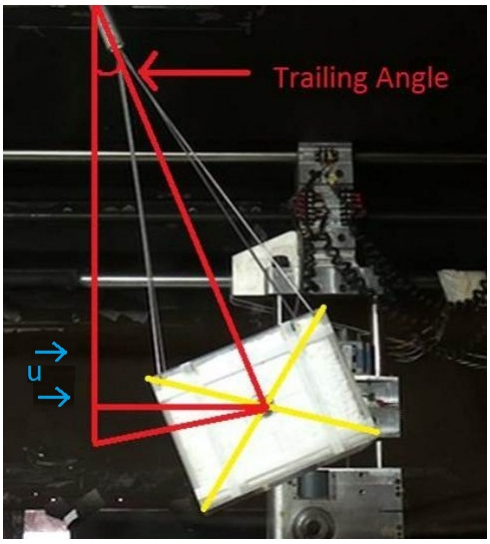

FIGURE 1. CONEX WIND TUNNEL TEST VIDEO ANALYSIS.

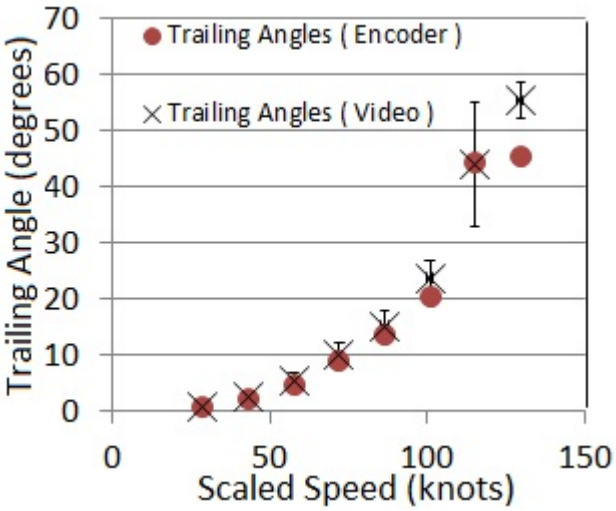

FIGURE 2. COMPARISON OF VIDEO ANALYSIS AND ENCODER DATA.

actual helicopter starting in hover and accelerating.

Divergence is defined as a condition where the amplification rate is above a certain threshold, or the amplitude of oscillations exceeds a specified threshold, either case being one that begins to cause concerns about the safety of the rotorcraft. These are subjective definitions and the air crew must exercise discretion and judgement. Good guidance on the mechanisms that are in play would enable techniques to be developed to either alleviate the amplification or quantitatively determine when safety becomes an issue.

TABLE 2. BASIC MECHANISMS FOR AMPLIFICATION.

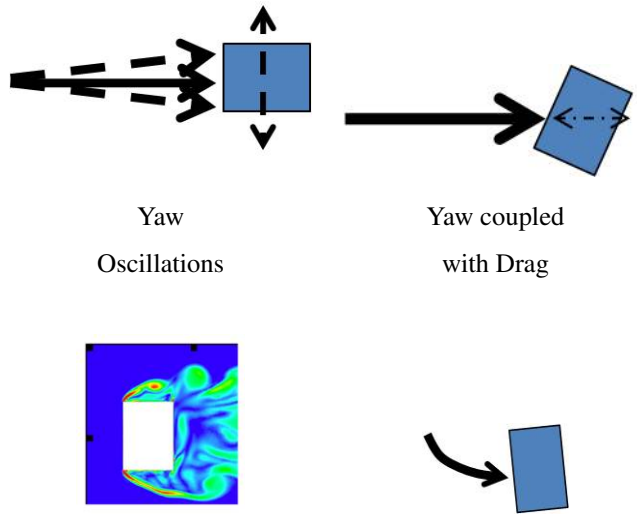

Basic Mechanisms for Amplification

Several basic mechanisms can be considered for the initiation of divergence. In each of these, different phenomena must reinforce the effect of each other, to amplify the motion. These are listed below and illustrated in Tab. 2.

1. Yaw oscillations induced by:
   (a) lateral swinging of the load
   (b) rotor wake swirl
   (c) helicopter manuever which causes an asymmetric C_p
2. Yaw oscillations can also couple with pitch through the action of drag forces that create fore-aft swing.
3. Yaw and lateral swing induced by vortex shedding.
4. Helicopter maneuver also affects vortex shedding, which in turn amplifies yaw and lateral motion.
5. Vortex shedding drives periodic drag oscillations, coupling angle of attack with yaw.

Demonstration Sequence

A demonstration sequence was developed to computationally simulate the different degrees of freedom in the motion of

the tethered box. The sequence consists of a step-by-step approach where motion from one degree of freedom is simulated before adding on further degrees of freedom. This model stays in the realm of rigid bodies and does not take into account the deformation of the body. For simplicity, the body is hinged at a point not at its center of mass and is considered as a compound pendulum. The model accounts only for one single sling that is attached to the center of the top surface of the box unlike the wind tunnel experiments where the box had four slings. To analyze the system, the conservation of angular momentum for a rigid body in two dimensional motion is used.

$$I_{zz}\alpha = I_{zz}\ddot{\theta} = \sum M_P - \overrightarrow{r_{pc}} \times m_T a_p \tag{1}$$

If the pivot point is taken to be P, then the equation simplifies to:

$$I_{zz}\ddot{\theta} = \sum M_P \tag{2}$$

$$I_{zz}^P \alpha = -mglsin(\theta) \tag{3}$$

The computation in this demonstration is done through MATLAB and SIMULINK models.

Case 1. Pendulum + Doublet + Freestream, no walls. The first case is to simulate the harmonic motion of a pendulum $\left(\frac{d^2\theta}{dt^2} + \frac{g}{l}sin\theta = 0\right)$ in the presence of a doublet and a freestream. The doublet is placed at the present location of the box/pendulum and acts as a circular body in the flow when a freestream is added. Mass and sling length of the tethered body are entered at the same values as used inthe CONEX wind tunnel experiments to maintain consistency. The body is subject to an initial condition of $\theta = 30^\circ$ where θ is the angle measured from the sling axis when the pendulum is at rest. As expected, the result shows harmonic motion from -30° to +30°.

Case 2. Case 1 + Mirror Images of Doublet (to simulate walls). In the second step of this demonstration, two imaginary doublets are added behind the actual physical location of the walls to mirror the doublet on the pendulum. Their location changes with the location of the center doublet and is determined at each step of the simulation in order to satisfy the boundary conditions at the wall. As the pendulum gets closer to one wall of the test section, doublets change their locations accordingly to maintain boundary conditions and simulate the effect of a physical wall. The doublet is a special case of a source-sink pair that leads to singularity. The model is designed with source-sink pairs on each wall and at the center of the blunt body. Each doublet provides two components of velocity. The components are separated into radial and orthogonal directions. Using the velocity potential due to a doublet, the velocity at a point is:

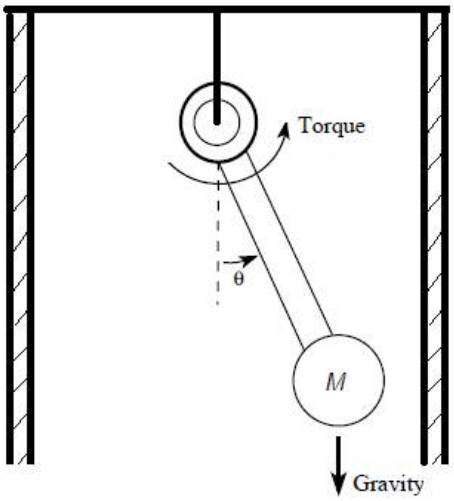

FIGURE 3. PENDULUM MODEL.

$$V_R = \left(U_\infty - \frac{k}{r^2}\right)\cos(\theta) \tag{4}$$

$$V_\theta = \left(-U_\infty - \frac{k}{r^2}\right)\sin(\theta) \tag{5}$$

Once the velocity is found, it is used to find the dynamic pressure at each side of the box. Using the stagnation pressure, flow is assumed to be isentropic, static pressure is solved for. This allows for finding out the force due to the induced velocity at each point and thereby leading to the forcing function due to the wall. Note that the velocity of the swinging pendulum motion is very small compared to the freestream velocity.

In this model, there are six different velocities that must be accounted for both faces (facing the wall) of the blunt body. After calculating the dynamic pressure due to each of the velocities, a force for each face (facing the wall) is calculated. Here dynamic

pressure, $q = \frac{1}{2}\rho V^2$. This force is then put into a form of linear momentum and then added to the differential equation governing the motion of the pendulum. The equation thus becomes:

$$I_{zz}^{P}\alpha = l \cdot F - mglsin(\theta) \tag{6}$$

The sign of F determines whether the force will be added or subtracted from the harmonic motion due to mass of the box.

It is seen from simulations that the wall force amplitude is constant throughout the time of the simulation; it is equal in magnitude and opposite in direction periodically and hence should not contribute any resultant force on the pendulum-like motion. This fact is reaffirmed by the results from the Simulink model simulation of the pendulum motion.

Case 3. Pendulum + Out of Phase Force (to simulate yaw). In the third step of the demonstration yaw oscillations are simulated in the absence of a force due to the mirrored doublets. This accounts for the case where the box is allowed to roll freely due to the harmonic pendulum motion and is subject to a yawing oscillation. The idea is to simulate a yawing force which is at the same frequency but out of phase with the pendulum motion. A Fast Fourier Transform (FFT) analysis is done on the pendulum motion from the first step to calculate that the frequency is 0.2489 rad/s. This frequency is introduced in the Simulink model by the use of a sine wave generator block which is given by:

$$y(t) = 0.0001Sin\left(2\pi(0.2489) + \frac{\pi}{2}\right) \tag{7}$$

The amplitude of this out of phase force relative to that of the primary wall effect force, has a critical effect on the stability of the pendulum motion. An amplitude of 0.0001 was found by trial and error to achieve an amplifying response that did not blow up (diverge off scale and stop the simulation) before 50 seconds. The appropriate range of amplitudes from aerodyamic loads must await further investigation, by correlation with quasi-steady load data from the wind tunnel and CFD, as well as correlation with the video data of the wind tunnel tests in the 42 inch wind tunnel. These efforts are left to continuing work. Figure 4 shows the amplifying response of the pendulum motion with time.

Case 4. Case 3 + Walls. In the fourth step in this demonstration, two degrees of freedom for the pendulum are introduced by adding the moment due to the force exerted by the mirrored

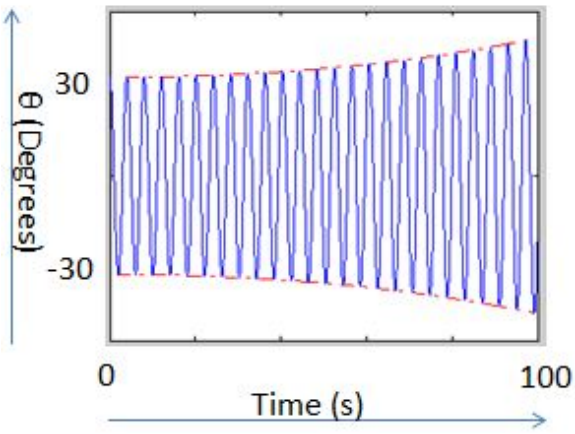

FIGURE 4. AMPLIFICATION OF THE PENDULUM MOTION WHEN COUPLED WITH AN OUT-OF-PHASE FORCE, WITH NO WALLS.

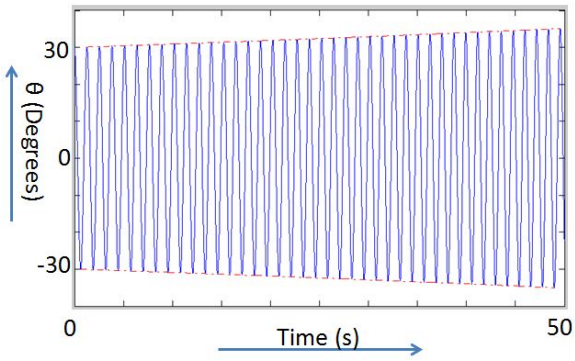

FIGURE 5. AMPLIFICATION OF THE PENDULUM MOTION OF A DOUBLET IN A FREESTREAM, WHEN COUPLED WITH AN OUT-OF-PHASE FORCE, WITH WALLS PRESENT.

doublets as well as an out of phase forcing function to simulate the yaw oscillations. For convenience, the derivative block is used to model the out of phase character of the yaw oscillations for this harmonic case. This case again showsin Fig. 5 an amplification in the oscillatory motion of the pendulum. It confirms the involvement of forces due to the wind tunnel walls with periodic yaw oscillations to create an amplification of roll oscillations.

Case 5. Wind Tunnel Blockage Metrics. This step is repeated for varying wind tunnel test section widths and box width to capture the change in amplification, as measured by the peak amplitude of oscillation at 50 seconds, starting with the same 30-degree initial condition in each run. Then two other cases are run to see if there is a relation between the flatness of the bluff body and the wall effect on amplification. Flatness of the body is defined as:

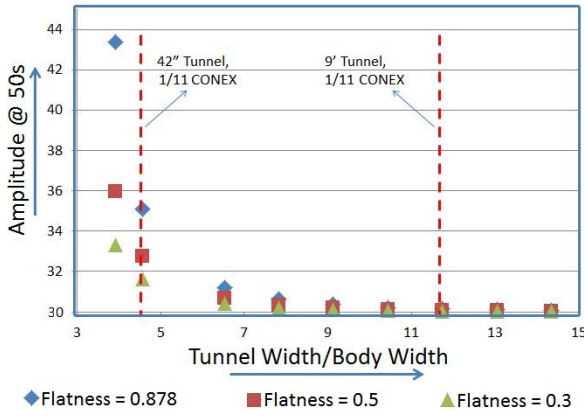

FIGURE 6. A DOUBLET IN A FREESTREAM WHEN COUPLED WITH AN OUT-OF-PHASE FORCE WITH WALLS PRESENT.

$$flatness = \frac{A_{ref}}{PlanformArea} = \frac{A_{ref}}{Length * Depth} \tag{8}$$

where A_{ref} is the area of the box facing the wall.

Hence, to consider the case of a flat plate, flatness will be close to zero whereas for a box the flatness ≥ 1.

From Fig. 6 it can be seen that at time t = 50 seconds, the amplitude of pendulum motion is higher in the case of the 42" wind tunnel as compared to the John J. Harper Wind Tunnel facility (test section width of 9 feet).

Comparison to Experimental Data

Videotapes of testing done with a 1/11 scale CONEX container in two wind tunnels were analyzed. In the case of the John Harper Wind Tunnel with a 7 ft x 9 ft test section, the model yawed 90 degrees in the speed range from 35-40 mph. It changed from an orientation where the narrow side faced the airflow, to one where the broad side faced the airflow. The model remained steady below and above this speed, with instabilities occurring at considerably higher speed. In the case of the 42 inch wind tunnel the model started spinning and rolling slowly at 10 mph. It then transitioned from narrow side windward, to broadside windward, at 15 mph. By averaging the frequencies of oscillation at different speeds in the video footage of the 42 inch wind tunnel, the frequency of the roll oscillations was computed as 3.7 radians per second. After computing the results of Case 5 with the parameters (such as moment of inertia of the load, sling length, distance from the walls etc.) used in the 42 inch wind tunnel, the pendulum frequency of roll oscillation was calculated to be 4.51 radians per second. This frequency is approximately 20% greater than the roll frequency observed in the experiment.

The video analysis of the 42 inch tunnel data shows the strong role of yaw-roll coupling in the behavior of the CONEX model. Near 15 mph, slow yaw begins, going past 90 degrees to switch to the broad-side-forward orientation. Overshoot of yaw results in a yaw oscillation at roughly half the frequency of the roll oscillation, reaching the extremes of yaw amplitude at the extremes of the pendulum swing, i.e., closest to the walls. It appears at this point that the effect of roll-yaw coupling at these initial stages may be more due to the asymmetric aerodynamics of the yawed box driving side force and hence roll oscillations. These results suggest that coupling with yaw changes the frequency from that predicted for a pure gravitational pendulum swing. However, note that no such oscillation is seen in the case of the 7 foot x 9 foot tunnel, where the 90 degree yaw transition occurs at 35-40 mph without appreciable overshoot.

At higher speeds, the roll-yaw roll also contributes to pitch oscillation, so that the model describes an approximately conical oscillation. This oscillation does amplify, until the model hits the walls at above 30 mph. Thus it appears that modeling the pitch oscillation (caused by the drag difference as the model yaws) may be needed in order to capture the full extent of amplification in the simulation. This is left to future work. The present simulation results show that there exist some combinations of roll and yaw, even at the same frequency, that will amplify when walls are present. The criteria developed for wall proximity to drive amplification provide initial guidance to design wind tunnel tests that are free of wall effects until large amplification occurs due to other mechanisms.

CONCLUSIONS

In this paper, a sequence of simple mathematical simulations is used to illustrate how to simulate the basic mechanisms by which a slung load may go into divergent oscillations. A compound pendulum representation of a slung load is modelled in a wind tunnel using potential flow around a doublet in a freestream, with the method of images used to represent tunnel walls. Importantly, this level of simulation is seen to provide guidance on the effects of tunnel walls in amplifying the oscillations that occur with a slung load.

1. The flow between the box and the tunnel walls produces a suction which in turn produces a force on the box. When there is only one degree of freedom, this suction is symmetric and does not contribute to instability.
2. Two degrees of freedom are present, a lateral swing and a forcing function that is out of phase with the lateral swing lead to divergence in the motion of the box. It is the interaction of the two that leads to an instability mode and the box

shows stable behavior in the case of one degree of freedom.

3. Although forces due to dynamic pressure exerted by the walls are sinusoidal, they lead to an increase in the amplitude of motion. Amplification rate is seen to be different for change in distance between the mirrored doublet.
4. The ratio of object width to test section width may impose a more stringent wall effect criterion than the 5% area blockage criterion that is currently employed in wind tunnel experiments. The simulation of two degrees of freedom for a pendulum like motion results in different amplitude changes.
5. The simulation helps to explain the differences observed in the experimental results between the 9 feet tunnel test section and 42 inch tunnel test section.
6. A flatness factor giving the ratio of side area to planform area helps to gauge the wall effect for different types of models and shows that a thicker model such as a box will suffer greater wall effects on aplification than a thin plate-like model, as expected.
7. Such a basic simulation framework shows promise to provide physical insight into slung load instability mechanisms, when the more complex pressure distributions and sling dynamics are systematically introduced into the simulation in continuing work.
8. Analysis experimental results from the smaller tunnel suggests that the amplification due to wall effect occurs when there is a subharmonic yaw oscillation coupling with the roll oscillation. Larger amplification occurs when there is pitch, roll and yaw coupling.

ACKNOWLEDGEMENTS

This work is part of Task 10 of the Vertical Lift Rotorcraft Center of Excellence project at Georgia Tech, funded by the US Army and NASA. The first author gratefully acknowledges the President's Undergraduate Research Award from Georgia Tech. Several students of the Experimental Aerodynamics Group at Georgia Institute of Technology assisted in the measurements and computation aspects related to this project. This work has been partially funded by the US Army/Navy/NASA Vertical Lift Rotorcraft Center of Excellence at Georgia Tech. The technical monitor is Dr. Michael Rutkowski. The views and conclusions contained in this document are those of the authors and should not be interpreted as repre- senting the official policies, either expressed or implied, of the U.S. Government. The U.S. Government is authorized to reproduce and distribute reprints for Government purposes notwithstanding any copyright notation thereon.

REFERENCES

[1] , 2003. Multiservice Helicopter Sling Load: Single-Point Load Rigging Procedures. AFJMAN 11-223, VOL II, FM 10-450-4, MCRP 4-23E, VOL II, September.

[2] Hoerner, S., 1965. *Fluid-Dynamic Drag*. Hoerner Fluid Dynamics, Brick Town, NJ.

[3] Wei, C., and Chang, J., 2002. "Wake and base-bleed flow downstream of bluff bodies with different geometry". *Experimental Thermal and Fluid Science,* ***26***, pp. 39–52.

[4] Nakamura, Y., 1993. "Bluff-body aerodynamics and turbulence". *Journal of Wind Engineering and Industrial Aerodynamics,* ***49***, pp. 65–78.

[5] Lee, B., 1990. "Some Observations of the Effect of Aspect Ratio on the Influence of Turbulence on the Drag of Rectangular Cylinders". *Journal of Wind Engineering and Industrial Aerodynamics,* ***33***, pp. 107–111.

[6] Gerrard, J., 1966. "The Mechanics of the Formation Region of Vortices Behind Bluff Bodies". *Journal of Fluid Mechanics,* ***25***, pp. 401–413.

[7] Barnes, F. H., and Grant, I., 1983. "Vortex shedding in unsteady flow". *Journal of Wind Engineering and Industrial Aerodynamics,* ***11***, pp. 335–344.

[8] Bearman, P., and Tombazis, N., 1993. "The effects of three-dimensional imposed disturbances on bluff body near wake flows". *Journal of Wind Engineering and Industrial Aerodynamics,* ***49***, pp. 339–350.

[9] Bentley, J., and Mudd, J., 2003. "Vortex shedding mechanisms in single and dual bluff bodies". *Flow Measurement and Instrumentation,* ***14***, pp. 23–31.

[10] King, R., 1977. "A Review of Vortex Shedding Research and Its Application". *Ocean Engineering,* ***4***, pp. 141–171.

[11] Komatsu, S., and Kobayashi, H., 1980. "Vortex-induced oscillation of bluff cylinders". *Journal of Wind Engineering and Industrial Aerodynamics,* ***6***, pp. 335–362.

[12] Matsumoto, M., 1999. "Vortex Shedding of Bluff Bodies: A Review". *Journal of Fluids and Structures,* ***13***, pp. 791–811.

[13] Micale, E. C., and Poli, C., 1973. "Dynamics of Sling Bodies using a Rotating Wheel for Stability". *Journal of Aircraft,* ***10***, pp. 80–86.

[14] Rosen, A., Cecutta, S., and Yaffe, R., 1999. "Wind Tunnel Tests of Cube and CONEX Models". *Technion Institute of Technology, Dept. of Aerospace Engineering, TAE,* ***844***.

[15] Theron, J., Gordon, R., Rosen, A., Cicolani, L., Duque, E., and Halsey, R., 2006. "Simulation of Helicopter Slung Load Aerodynamics: wind tunnel validation of two computational fluid dynamics codes". In Proceedings of the 36th AIAA Fluid Dynamics Conference.

[16] Cicolani, L., Raz, R., Rosen, A., Gordon, R., Cone, A., Theron, J., Lusardi, J., Tischler, M., and Robinson, D., 2007. "Flight Test, Simulation and Passive Stabilization of a Cargo Container Slung Load in Forward Flight". In Annual Forum Proceedings of the American Helicopter Society, Vol. 63, p. 2177.

[17] Raz, R., Rosen, A., Carmeli, A., Lusardi, J., Cicolani, L.,

and Robinson, D., 2010. "Wind Tunnel and Flight Evaluation of Passive Stabilization of a Cargo Container Slung Load". *Journal of the American Helicopter Society,* ***55***, p. 032001.

[18] Reddy, K., Truong, T., Stuckey, R., and Bourne, K., 2007. "Dynamic simulation of a helicopter carrying a slung load". In Proceedings of MODSIM07, International Congress on Modelling and Simulation. Modelling and Simulation Society of Australia and New Zealand, International Congress on Modelling and Simulation. Modelling and Simulation Society of Australia and New Zealand, L. Oxley and D. Kulasiri, eds., no. Paper 49 s11, Modelling and Simulation Society of Australia and New Zealand Inc, pp. 2740–2746. Defence Science and Technology Organisation, Australian Department of Defence.

[19] Cicolani, L., and Kanning, G., 1986. General equilibrium characteristics of a dual-lift helicopter system. TP 2615, NASA.

[20] Greenwell, D., 2011. "Modelling of static aerodynamics of helicopter underslung loads". *Aeronautical Journal,* ***115***(1166), pp. 201–219.

[21] Mantri, R., Raghav, V., Komerath, N., and Smith, M. J., 2011. "Stability prediction of sling load dynamics using wind tunnel models". In Proceedings of the American Helicopter Society 67th Annual Forum.

[22] Raghav, V., Mantri, R., Komerath, N., and Smith, M., 2011. "Study of factors driving pitch, roll and yaw coupling in bluff body aerodynamics". In AIAA Applied Aerodynamics Conference.